Smart Mater. Struct. 24 (2015) 025039 (15pp)

Charge, voltage, and work-conversion formulas for magnetoelectric laminated composites

T.I. Muchenik and E.J. Barbero[1],
West Virginia University, Morgantown USA

Abstract

A novel analytical model for *magnetoelectric* (ME) laminate composites made of *piezoelectric* (PE) and *piezomagnetic* (PM) phases is proposed. The multiphysics equations are applied to all four possible laminate configurations (TT, LT, TL, and LL), with appropriate boundary conditions. Closed form, explicit formulas are derived for the calculation of the intrinsic ME charge coefficient, ME voltage coefficient, and ME coupling factor as a function of material properties of both phases and the PM volume fraction. The predicted ME voltage coefficient is in agreement with previous work and experimental data. A new approach is proposed to take into account the conductivity of the PM phase resulting in calculated ME charge coefficients within 30% of experimental data, which is a major departure from the available approaches that either require to impose an additional constraint on the model or simply ignore the conductivity of the PM phase. To assess the conversion of magnetic work into electric work , a novel approach is developed to calculate the ME coupling factor in closed form by using the calculated properties of the ME composite structure, thus avoiding the equivalent circuit assumption, and furthermore novel coupling factor formulas are developed for all four polarization/magnetization configurations and taking into account the strain coupling in both inplane directions. Using actual material properties, conclusions are drawn regarding the optimal configuration and PM volume fraction necessary to achieve maximum charge, voltage, and work conversion.

Keywords

Piezoelectric, Piezomagnetic, Magnetostrictive, Magnetoelectric, Composite, Modeling

[1]Corresponding author: ever.barbero@mail.wvu.edu.
The final publication is available at http://dx.doi.org/10.1088/0964-1726/24/2/025039

1 Introduction

Interest in *magnetoelectic* (ME) devices is motivated by potential applications such as sensors [1], energy harvesters [2–8], and solid state memory [9]. Although ME materials exist in nature [10], their ME charge coefficient β is too small ($4.13ps\ m^{-1}$ [2] at 2°K [11]) and/or their Néel temperature is too low for practical applications.

On the other hand, composite materials can be built to exploit the product property between a strongly *magnetostrictive* (MS) s/H material and a strongly *piezoelectric* (PE) E/s material; that is, obtaining the product ME property E/H, where s, H, E, are the strain, magnetic filed, and electric field, respectively. Unlike naturally occurring ME materials, ME composites can achieve very strong ME voltage coefficients ($\alpha = 5.76V\ A^{-1}$ [3] [12], which corresponds to $\beta \sim 13000ps\,m^{-1}$) at room temperature. Therefore, ME composites are considered to be *metamaterials* [13].

While particulate composites are limited in performance by atomic diffusion, mechanical defects, and leakage currents, laminated composites may overcome or minimize these problems [12, 14, 15]. Since the constituent PE and MS materials, and the laminated composite they form, all have other useful properties such as the ability to carry loads (stiffness and strength), ME composites may be considered to be *multifunctional* materials as well.

PE materials display an approximately linear strain-electric field response over a wide range of strain or electric fields. On the other hand, MS materials display a nonlinear strain-magnetic field (s-H) response. However, most applications use these materials over a small magnetic-field range centered around a large, fixed magnetic bias. As a result, the behavior may be approximated as linear, and in this later case the material is said to be *piezomagnetic* (PM). The nonlinearity of the magnetic properties of the MS phase is outside the scope of this work.

Analytical models [16–19] are useful because they can be used to quickly predict approximate values for the expected voltage, charge, or work conversion of the device as a function of material properties for the PE and PM materials as well as a function of the relative thicknesses, or volume fractions of the constituents. Therefore, an analytical model for ME laminate composites made of PE and PM layers is developed herein. The governing equations are applied to all four possible laminate configurations (TT, LT, TL, and LL), with appropriate boundary conditions. The system of equations is solved using Wolfram Mathematica [20]. Conclusions are drawn regarding the merits, drawbacks, and requirements for analysis of each configuration.

Closed form, explicit formulas are derived for the calculation of the ME voltage coefficient α as a function of the material properties of PE and PM phases, and the PM volume fraction, χ. The predicted ME voltage coefficient is in agreement with previous work and experimental data.

Also, closed form, explicit formulas are derived for the calculation of the ME charge coefficient β as a function of the material properties of PE and PM phases, and the PM volume fraction. The values of ME charge coefficient previously calculated in the literature do not agree with available experimental data. This is due to the fact that the high con-

[2] $C\,A^{-1}m^{-1} = s\,m^{-1}$

[3] $V\,A^{-1} = 796mV\,cm^{-1}Oe^{-1}$

ductivity of the PM phase has not being taken into account in previous models [18], giving predictions three orders of magnitude smaller than experimental values. A new approach is proposed in this work (§ 2.2) to take into account the conductivity of the PM phase, resulting in calculated ME charge coefficients within 30% of experimental data. The new proposed approach does not require to impose the additional constraint of zero electric field in the PM phase. While this would be acceptable for the particular case of laminates, it would not apply to more general cases. For example, such constraint would imply that a finite element implementation for arbitrary shape of PE inclusions in a PM matrix would have to be programmed with two different element formulations; one with the correct constitutive equation (2) for the PE phase and another with E=0 for the PM phase, thus canceling (2). To avoid such inconsistency and lack of generality, a new approach is proposed within the context of electrostatics, magnetostatics, and elasticity; that is, without requiring the addition of electrodynamics, which would increase the complexity of the constitutive equations significantly.

The ME voltage coefficient provides a indication of the ME material's performance to produce an electric field E, and thus voltage $V = E\,t$ from exposure to a magnetic field H, when no work is drawn from the device[4]. This definition may lead to maximum ME voltage performance when the volume fraction of PM phase $\chi \to 1$, but a nearly zero thickness of PE would produce almost no work and thus make it difficult to measure the voltage.

Similarly, the ME charge coefficient represents the performance of the ME material to produce an electric displacement D, and thus charge $Q = D\,A$ (where A is the area of the device) from exposure to a magnetic field H, again when no work is drawn from the device. This definition may lead to maximum ME charge performance when the volume fraction of PM phase $\chi \to 1$, but a nearly zero thickness of PE would produce almost no work and thus make it very difficult to measure the charge Q or current $I = \int Q\,dt$.

The ME coupling factor κ yields a measure of the ME material's performance to convert magnetic work into electric work [21, 22]. This coefficient has been calculated in [21] only for the push-pull configuration, and only the mechanical coupling in the direction of the applied magnetic field was considered. Furthermore, an equivalent circuit for the composite had to be assumed in [21]. In this work, closed form, explicit formulas are derived for the calculation of the ME coupling factor as a function of the material properties of PE and PM phases, and the PM volume fraction considering mechanical coupling in all directions, without the need to assume an equivalent circuit.

The formulas for these coefficients require calculation of the dielectric permittivity of the device ϵ^H at constant magnetic field, H, and magnetic permeability of the device μ^E at constant electric field, E. The well known series/parallel capacitor formulas are not appropriate for PM devices because the application of a magnetic field results in an electrical displacement and vice versa, due to the inherent coupling present in the device. Thus, a methodology for the calculation of these coefficients is proposed, which is then used to derive close form, explicit formulas for their calculation.

This work is concerned with predicting the intrinsic material properties of the composite, while the extrinsic properties are those that can be measured in an experimental setup. The

[4]Where t is the total thickness of the device, E is the average electric field over t, and V is the voltage measured across the thickness t of the device.

difference between intrinsic and extrinsic can be calculated by established formulas for the demagnetizing effect [23, 24].

Three materials, LSMO/PZT, FeBSiC/PZN-PT, and Terfenod-D/PZT-5H are used to illustrate salient aspects of the model, of the various configurations, and of the three coefficients. Application of the proposed formulas highlights a trade off between deformation and charge/voltage/work as a function of PM volume fraction.

2 Model description

The analytical model is based in the following constitutive equations:

$$s = S\sigma + d^T E + q^T H \tag{1}$$

$$D = d\sigma + \epsilon E \tag{2}$$

$$B = q\sigma + \mu H \tag{3}$$

where σ is the stress tensor, s is the strain tensor, E is the electric field vector, H is the magnetic field vector, D is the electric displacement vector, B is the magnetic flux density vector, S is the compliance tensor (measured at constant electric and magnetic field), ϵ is the dielectric permittivity tensor (measured at constant stress), μ is the magnetic permeability tensor (measured at constant stress), d is the PE charge constant tensor, and q is the PM constant tensor. These equations describe the behavior of the PM and PE phases. As it was discussed before, all the materials used as a PM are actually magnetostrictive with a nonlinear relationship between strain and magnetic field, but they are customarily treated as linear in the close neighborhood of an applied *magnetic bias*. Then, the PM constant tensor and all the PM properties are measured at this magnetic bias.

In this work the materials are assumed to be transversally isotropic. For PE and PM materials the axis of symmetry is the direction at which the material is polarized or magnetized, respectively. However, for sake of expedience, this direction is simply called the *polarization (or magnetization) direction*. Further, it is convenient to define a material coordinate system were the 3-direction is aligned with the polarization (or magnetization), see Figure 1. Since each phase can be polarized, or magnetized, in different directions, the global coordinate system of the composite may not coincide with the material coordinate system.

The compliance tensor S is then defined as follows (Equation 1.92 from [25]):

$$S = \begin{bmatrix} S_{11} & S_{12} & S_{23} & 0 & 0 & 0 \\ S_{12} & S_{11} & S_{23} & 0 & 0 & 0 \\ S_{23} & S_{23} & S_{33} & 0 & 0 & 0 \\ 0 & 0 & 0 & S_{44} & 0 & 0 \\ 0 & 0 & 0 & 0 & S_{44} & 0 \\ 0 & 0 & 0 & 0 & 0 & 2(S_{11} - S_{12}) \end{bmatrix} \tag{4}$$

The PE charge constant tensor d is defined as

$$d = \begin{bmatrix} 0 & 0 & 0 & 0 & d_{15} & 0 \\ 0 & 0 & 0 & d_{15} & 0 & 0 \\ d_{31} & d_{31} & d_{33} & 0 & 0 & 0 \end{bmatrix} \tag{5}$$

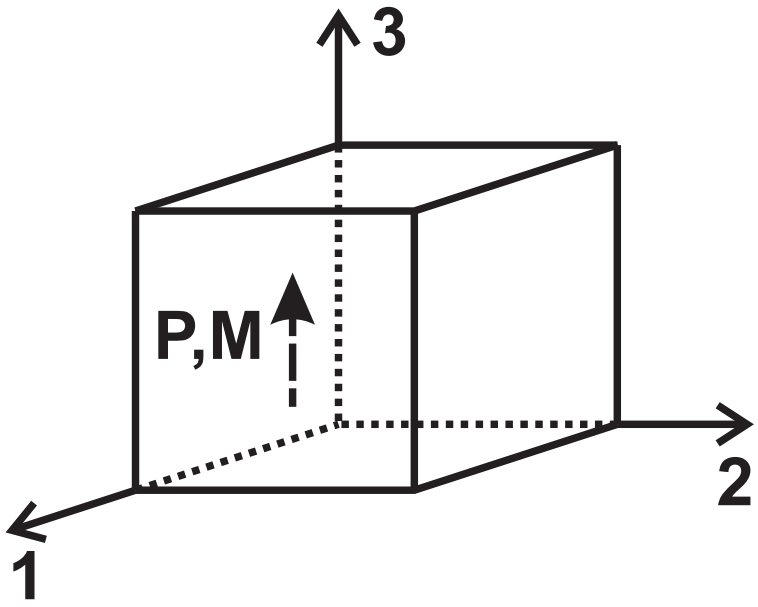

Figure 1: Material coordinate system.

where

$$d_{ij} = \frac{s_j}{E_i}\Big]_{\sigma=0} = \frac{D_i}{\sigma_j}\Big]_{E=0} \tag{6}$$

The PM constant tensor q is defined in the same way, where

$$q_{ij} = \frac{s_j}{H_i}\Big]_{\sigma=0} = \frac{B_i}{\sigma_j}\Big]_{H=0} \tag{7}$$

The dielectric permittivity ϵ, and magnetic permeability μ, are diagonal tensors defined as

$$\epsilon = \epsilon_{ij}\delta_{ij} \tag{8}$$

$$\mu = \mu_{ij}\delta_{ij} \tag{9}$$

where δ_{ij} is the Kronecker symbol and x_3 is the axis of transverse isotropy, which coincides with the direction of polarization or magnetization ($\epsilon_{11} = \epsilon_{22}$ and $\mu_{11} = \mu_{22}$).

ME devices can be built using four different configurations (Figure 2): transverse magnetization with transverse polarization (TT), longitudinal magnetization with transverse polarization (LT), transverse magnetization with longitudinal polarization (TL), and longitudinal magnetization with longitudinal polarization (LL). For simplicity, only two layers are shown in Figure 2, but it is assumed that the actual device is symmetrically laminated. Furthermore, the laminas are thin in comparison to the in-plane dimensions, resulting in a state of plane stress [25] and insignificant shear lag effect [23]. As a result, the stresses considered in this work are averaged through the thickness of each lamina and the intralaminar/interlaminar shear strains are negligible [25]. Consequently, the ME pair is assumed to be fully effective over its entire area.

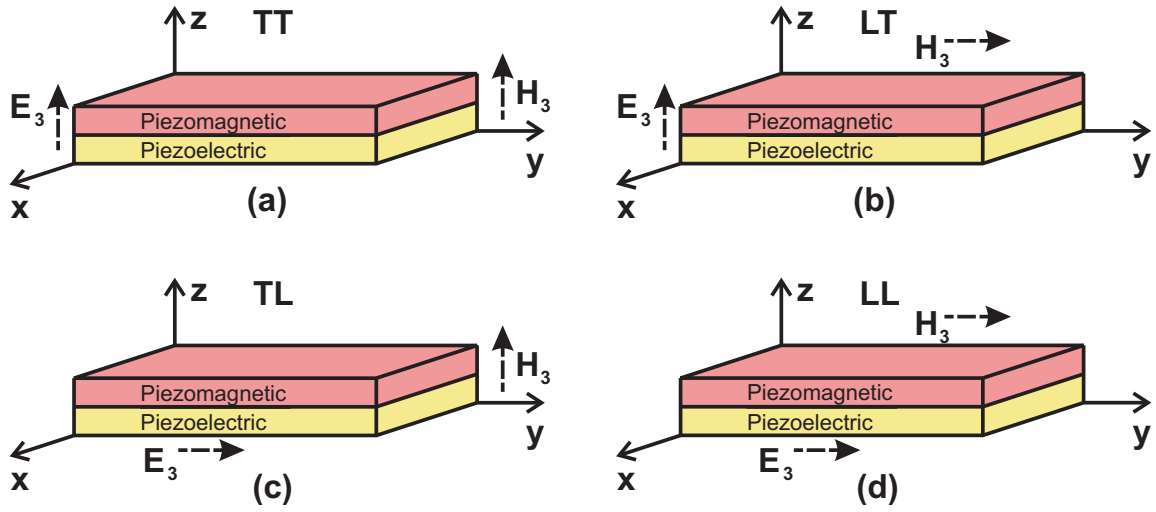

Figure 2: Laminate configurations: (a) transverse magnetization and transverse polarization (TT), (b) Longitudinal magnetization and transverse polarization (LT), (c) transverse magnetization and longitudinal polarization (TL), and (d) longitudinal magnetization with longitudinal polarization (LL).

The PE phase is most commonly polarized in the transverse direction. Otherwise, an insulator is needed at the interface to prevent charge leakage from the PE through the PM phase, since the latter is highly conductive. For example, a longitudinally polarized PZT was bonded to two magnetostrictive FeBSiC alloy (Metglas) foils, using two Kapton films in between to avoid leakage [26]. In this way, the electric field is confined to the PE phase.

The four possible geometric configurations shown in Figure 2 (a), (b), (c) and (d) are implemented by appropriate boundary conditions, as follows.

2.1 Transverse magnetization and polarization (TT)

Using (1) for the first term of the strain vector, yields

$$s_x = \sigma_x(S_{11} + S_{12}) + d_{31}E_z + q_{31}H_z \tag{10}$$

where $\sigma_x = \sigma_y$ because of the symmetry of the applied fields and geometry, $\sigma_z = 0$ because the laminate is not restrained to deform in the z-direction. Also, PE and PM are polarized (magnetized) in the z-direction shown in Figure 2.a. Equation (10) is valid for both PM and PE phases. Since $d_{31}^{PM} = 0$ in the PM phase, (10) reduces to

$$s_x^{PM} = \sigma_x^{PM}(S_{11}^{PM} + S_{12}^{PM}) + q_{31}^{PM}H_z^{PM} \tag{11}$$

Since $q_{31}^{PE} = 0$ in the PE phase, (10) reduces to

$$s_x^{PE} = \sigma_x^{PE}(S_{11}^{PE} + S_{12}^{PE}) + d_{31}^{PE}E_z^{PE} \tag{12}$$

From (2), the electric displacement in the z-direction, D_z, is expressed as

$$D_z = 2d_{31}\sigma_x + \epsilon_{33}E_z$$

Since $d_{31}^{P}M = 0$ in the PM phase

$$D_z^{PM} = \epsilon_{33}^{PM} E_z^{PM} \tag{13}$$

and for the PE phase

$$D_z^{PE} = 2d_{31}^{PE}\sigma_x^{PE} + \epsilon_{33}^{PE} E_z^{PE} \tag{14}$$

Using the same approach the magnetic flux density in the z-direction for the PM phase is

$$B_z^{PM} = 2q_{31}^{PM}\sigma_x^{PM} + \mu_{33}^{PM} H_z^{PM} \tag{15}$$

and the magnetic flux density for the PE phase is

$$B_z^{PE} = \mu_{33}^{PE} H_z^{PE} \tag{16}$$

Assuming that the PE and PM layers are perfectly bonded, the strain in the x and y-direction on both layers are equal

$$s_x^{PE} = s_x^{PM} \tag{17}$$

By force equilibrium, the force in the PM and PE phases have the same magnitude and opposite direction. The PM volume fraction, χ, is defined to take into account laminae with different thicknesses

$$\chi = \frac{V^{PM}}{V^{PM} + V^{PE}}$$

where V is the volume of each phase. Then, the equilibrium of forces is expressed as

$$\sigma_x^{PM} = -\sigma_x^{PE}\left(\frac{1}{\chi} - 1\right) \tag{18}$$

To produce an electric displacement, D, charge has to flow in the laminate of a certain area. Since the charge can only flow from the top to the bottom electrode, the electric displacement, D, is the same in the PE and PM phases

$$D_z^{PM} = D_z^{PE} \tag{19}$$

The same applies to the magnetic flux density

$$B_z^{PM} = B_z^{PE} \tag{20}$$

Since the applied magnetic field and the measured electric field are average values, it is convenient to define the following averages

$$E^{avg} = E_z^{PE}(1-\chi) + E_z^{PM}\chi \tag{21}$$

$$H^{avg} = H_z^{PE}(1-\chi) + H_z^{PM}\chi \tag{22}$$

The ME voltage coefficient is experimentally measured by applying a magnetic field to the composite and measuring the open circuit voltage ($D_z = 0$). The ME voltage coefficient, α, is an intrinsic property of the composite and is calculated by dividing the measured voltage by the thickness and the applied magnetic field. This can be mathematically expressed as

$$\alpha = \frac{V}{tH^{avg}}\Big]_{D=0} = \frac{E^{avg}}{H^{avg}}\Big]_{D=0} \tag{23}$$

where V is the voltage generated between the upper and lower electrode as a response of the applied magnetic field and t is the total thickness of the composite. The second equality is obtained by the definition of the electric field ($E = \frac{V}{t}$). In this work, the ME voltage coefficient for the TT configuration is calculated by solving the system of equations (11)–(23), resulting in the following formula

$$\begin{aligned} \alpha_{TT} &= \frac{A_1}{B_1} \\ A_1 &= -(2d_{31}^{PE}\mu_{33}^{PE}q_{31}^{PM}(\chi-1)\chi) \\ B_1 &= (2(d_{31}^{PE})^2\chi(\mu_{33}^{PM}+\mu_{33}^{PE}\chi-\mu_{33}^{PM}\chi)+\epsilon_{33}^{PE}(2(q_{31}^{PM})^2(\chi-1)^2 \\ &\quad -(\mu_{33}^{PM}(\chi-1)-\mu_{33}^{PE}\chi)(S_{11}^{PM}(\chi-1)+S_{12}^{PM}(\chi-1)-(S_{11}^{PE}+S_{12}^{PE})\chi))) \end{aligned} \tag{24}$$

which is available in MATLAB® and Scilab© format in the Website [27].

The ME voltage coefficient calculated in this work is compared to the results reported in [19]. Lead zirconate titanate (PZT) and lanthanum strontium manganite (LSMO) were used in [19] for the PE and PM phase, respectively. The properties used for these materials are reported in Table 1. The results obtained from the model proposed in [19] for different PM volume fractions are compared with the proposed model. The outcome can be seen in Figure 3, showing agreement between the models. The data shows a trade off between the volume of PE and PM phase with an optimum value of ME voltage coefficient at $\chi = 0.65$.

When higher volumes of PM phase are used (higher PM volume fraction χ), it gives higher strain, resulting in a higher electric field in the PE phase. The relationship between the electric field in the PE phase and the electric field in the composite can be seen in (21), showing that the total electric field depends on the electric field produced in the PE phase and the PM volume fraction (or thickness).

For PM volume fraction below the optimum, increasing the thickness of the PM phase gives an increase of the total electric field, which is stronger than the effect of the reduction of the thickness of the PE phase. But in the case of PM volume fraction above the optimum, even though the electric field in the PE phase increases with the increased thickness of PM phase, the decrease in PE phase thickness results in a decrease of the total electric field of the composite. Thus the parabolic response observed in Figure 3.

The ME charge coefficient β is experimentally measured by applying a magnetic field to the composite and measuring the short circuit charge with $E = 0$. The ME charge coefficient is an intrinsic property that is calculated as follows

$$\beta = \frac{Q}{AH^{avg}}\Big]_{E=0} = \frac{D^{avg}}{H^{avg}}\Big]_{E=0} \tag{25}$$

where Q is the charge generated in the direction of polarization and A is the total area of composite perpendicular to the polarization.

Material Property	LSMO	PZT	Units
S_{11}	15	15.3	$10^{-12}m^2N^{-1}$
S_{12}	-5	-5	$10^{-12}m^2N^{-1}$
ϵ_{33}/ϵ_0	10	1750	
μ_{33}/μ_0	2	1	
d_{31}	0	-175	$10^{-12}C\,N^{-1}$
d_{33}	0	400	$10^{-12}C\,N^{-1}$
q_{31}	250	0	$10^{-12}m\,A^{-1}$
q_{33}	-120	0	$10^{-12}m\,A^{-1}$

Table 1: Material Properties of PZT and LSMO from [19].

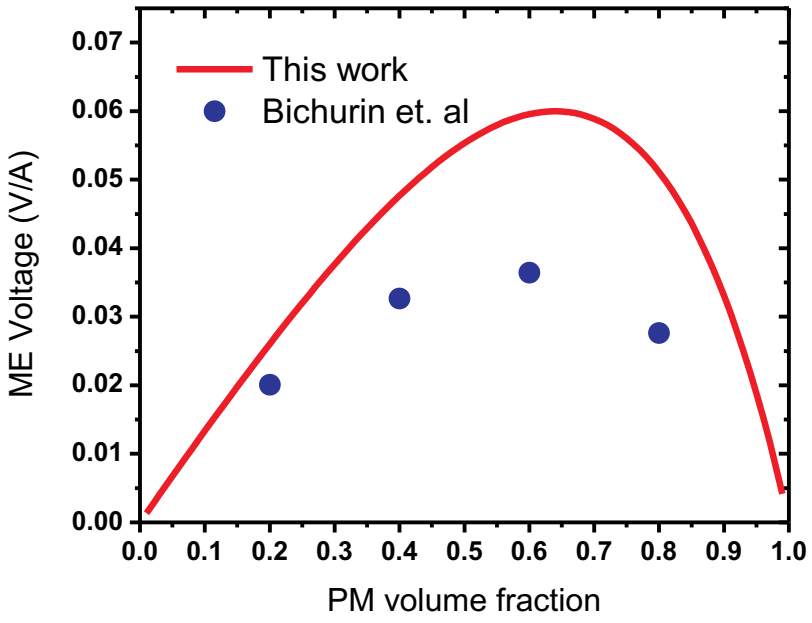

Figure 3: Comparison between the ME voltage coefficient obtained in this work and the work made by Bichurin *et al.* [19] for LSMO/PZT in TT configuration.

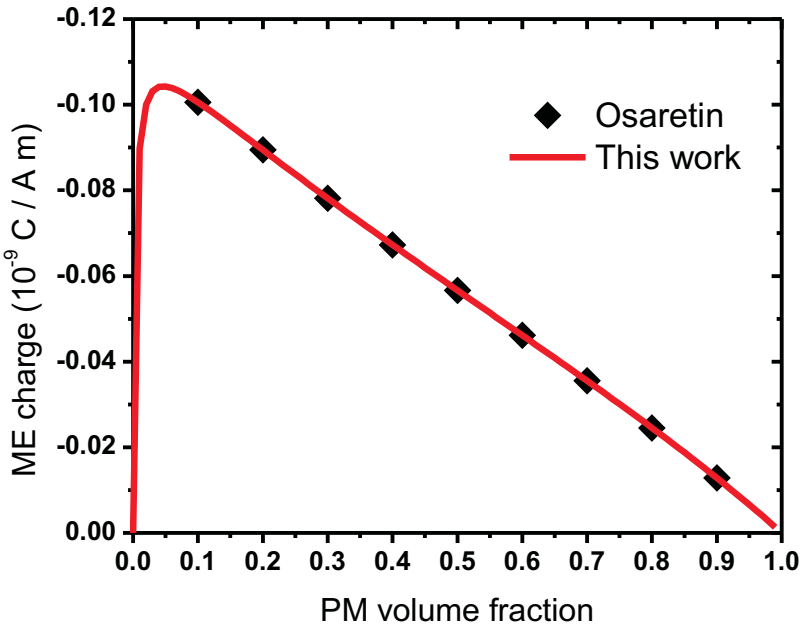

Figure 4: ME charge coefficient for different PM volume fractions of laminated CFO-PZT (TT) composite. The obtained results were compared with the work made by Osaretin [18].

An analytical expression for the ME charge coefficient in the TT configuration is obtained by solving the previous system of equations with the average electric field equal to zero, $E^{avg} = 0$, resulting in the following formula

$$\begin{aligned}
\beta_{TT} &= \frac{C_1}{D_1} \qquad (26)\\
C_1 &= (2d_{31}^{PE}\epsilon_{33}^{PM}\mu_{33}^{PE}q_{31}^{PM}(\chi-1)\chi)\\
D_1 &= (-\epsilon_{33}^{PM}(\chi-1)(2(q_{31}^{PM})^2(\chi-1)^2-(\mu_{33}^{PM}(\chi-1)-\mu_{33}^{PE}\chi)(S_{11}^{PM}(\chi-1)+S_{12}^{PM}(\chi-1)\\
&\quad -(S_{11}^{PE}+S_{12}^{PE})\chi))+\chi(2(d_{31}^{PE})^2\chi(\mu_{33}^{PM}+\mu_{33}^{PE}\chi-\mu_{33}^{PM}\chi)+\epsilon_{33}^{PE}(2(q_{31}^{PM})^2(\chi-1)^2\\
&\quad -(\mu_{33}^{PM}(\chi-1)-\mu_{33}^{PE}\chi)(S_{11}^{PM}(\chi-1)+S_{12}^{PM}(\chi-1)-(S_{11}^{PE}+S_{12}^{PE})\chi))))
\end{aligned}$$

The values obtained with this equation were compared with those obtained using Equation 16 in [18]. The results are shown in Figure 4. There is good agreement between the model proposed in [18] and the present work.

To calculate the ME charge coefficient, the electric field between electrodes is set to be zero as a boundary condition. If the total electric field is zero, it does not imply that the electric field in the PM phase and the PE phase are zero, as it can be seen in (21), but if the total electric field and the electric field in the PM phase are zero, the electric field in the PE phase will also be zero. In the proposed model, the electric field generated in the PM phase (E_z^{PM}) is considerably high. In real applications, the PM phase cannot sustain an electric field after a period of time because the electric conductivity of this material is high (the conductivity of CFO is $0.01 S\,cm^{-1}$) [28]. If the conductivity of the composite were to

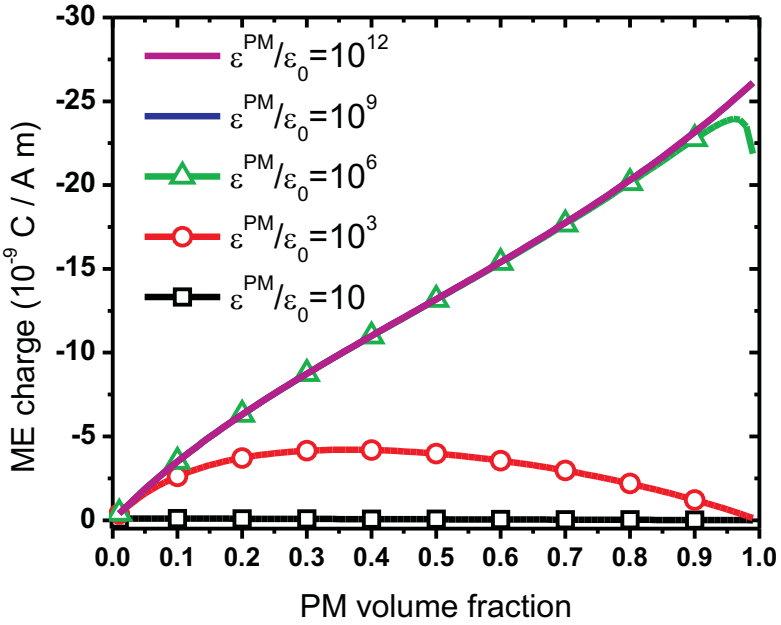

Figure 5: ME charge coefficient for different dielectric constants of the PM phase of the laminated CFO-PZT (TT) composite.

be modeled explicitly, the complexity of the model would increase significantly.

There are two ways to overcome this. First, the electric field in the PM phase can be set to be zero as an additional constraint condition ($E_z^{PM} = 0$). Second, the dielectric constant of the PM phase can be changed to avoid the generation of a electric field through the PM phase. As it can be seen in (13), in order to decrease the electric field generated in the PM phase, the dielectric constant of the PM phase, ϵ_{33}^{PM}, has to be increased. Both methods work equally well within the context of the model proposed herein but we wish to emphasize the fact that, unless the electric field in the PM phase is explicitly set to zero, the dielectric constant of the PM phase must be increased to a high value. Otherwise, model results will not be accurate, and sometimes this fact has been overlooked in the literature.

In the TT configuration, the magnetic field goes through both phases. The electric field goes through the PE phase and the associated electric displacement ($D^{PM} = \epsilon^{PM} E^{PM}$) goes through the PM phase. In other words, the fields are not confined to either phase. The equations reflect these facts.

The ME charge coefficients for different values of the dielectric constant of the PM phase are shown in Figure 5. The higher the dielectric constant of the PM phase, the higher the ME charge coefficient. This trend is observed until the dielectric constant reaches values of $\epsilon_{33}^{PM}/\epsilon_0 = 10^9$. Higher values have no significant effect.

2.2 Longitudinal magnetization and transverse polarization (LT)

The ME charge coefficient has been measured by several researchers. The results of the proposed model are compared with experimental data reported in [29], where two layers of FeBSiC alloy were bonded to a (100) oriented PZN-PT layer, with 33% PM volume fraction in an LT configuration. The experimental value of ME charge coefficient reported is $168 \times 10^{-9} C\, A^{-1} m^{-1}$. To compare this values with the current model, the analytical expressions for the LT configuration are obtained as follows.

To obtain the ME coefficients for the LT configuration, a similar approach to the TT configuration is used. Using (1) for the first and second terms of the strain vector in the PE phase, the following equations are obtained

$$s_x^{PE} = S_{11}^{PE}\sigma_x^{PE} + S_{12}^{PE}\sigma_y^{PE} + d_{31}^{PE}E_z^{PE} \quad (27)$$

$$s_y^{PE} = S_{12}^{PE}\sigma_x^{PE} + S_{11}^{PE}\sigma_y^{PE} + d_{31}^{PE}E_z^{PE} \quad (28)$$

In this case $\sigma_x \neq \sigma_y$ since the magnetic field applied in the y-direction will produce different strains in the x and y-direction. In the case of the PM phase, the first and second terms of the strain vector are

$$s_x^{PM} = S_{11}^{PM}\sigma_x^{PM} + S_{23}^{PM}\sigma_y^{PM} + q_{31}^{PM}H_y^{PM} \quad (29)$$

$$s_y^{PM} = S_{23}^{PM}\sigma_x^{PM} + S_{33}^{PM}\sigma_y^{PM} + q_{33}^{PM}H_y^{PM} \quad (30)$$

From (2), the electric displacement in the z-direction for the PE phase is expressed as

$$D_z^{PE} = d_{31}^{PE}\sigma_x^{PE} + d_{31}^{PE}\sigma_y^{PE} + \epsilon_{33}^{PE}E_z^{PE} \quad (31)$$

and the following equation is obtained for the PM phase

$$D_z^{PM} = \epsilon_{11}^{PM}E_z^{PM} \quad (32)$$

The same procedure is used to obtain the magnetic flux density in the y-direction for the PM phase

$$B_y^{PM} = q_{31}^{PM}\sigma_x^{PM} + q_{33}^{PM}\sigma_y^{PM} + \mu_{33}^{PM}H_y^{PM} \quad (33)$$

and for the PE phase

$$B_y^{PE} = \mu_{11}^{PE}H_y^{PE} \quad (34)$$

The strain in the x and y-direction are the same for the PM and PE layers, assuming they are perfectly bonded

$$s_x^{PE} = s_x^{PM} \quad (35)$$

$$s_y^{PE} = s_y^{PM} \quad (36)$$

By force equilibrium, the force produced be the PM phase restricted by the PE phase has the same magnitude and opposite directions

$$\sigma_x^{PM} = -\sigma_x^{PE}(\frac{1}{\chi} - 1) \quad (37)$$

$$\sigma_y^{PM} = -\sigma_y^{PE}(\frac{1}{\chi} - 1) \quad (38)$$

The electric displacement is the same in the PE and the PM phases because the charge is produced between the top and the bottom of the laminate

$$D_z^{PM} = D_z^{PE} \tag{39}$$

Since the magnetic field is applied in the y-direction, the magnetic field in each phase has to be equal

$$H_y^{PM} = H_y^{PE} \tag{40}$$

Again, it is convenient to define the averaged electric field, since this is the value which is externally measured:

$$E^{avg} = E_z^{PE}(1-\chi) + E_z^{PM}\chi \tag{41}$$

The ME voltage and charge coefficient is obtained by solving the system of equations (27)–(41) and setting the electric displacement equal to zero ($D_z = 0$)

$$\begin{aligned}
\alpha_{LT} &= \frac{A_2}{B_2} \qquad (42)\\
A_2 &= d_{31}^{PE}(\chi-1)\chi(q_{33}^{PM}((S_{23}^{PM}-S_{11}^{PM})(1-\chi)-(S_{11}^{PE}-S_{12}^{PE}))\chi)\\
&\quad +q_{31}^{PM}(S_{23}^{PM}(1-\chi)+S_{33}^{PM}(\chi-1)+(-S_{11}^{PE}+S_{12}^{PE})\chi)\\
B_2 &= (d_{31}^{PE})^2\chi(S_{11}^{PM}-2S_{23}^{PM}(1-\chi)+S_{33}^{PM}(1-\chi)-(-2S_{11}^{PE}+2S_{12}^{PE}+S_{11}^{PM})\chi)\\
&\quad \epsilon_{33}^{PE}((S_{23}^{PM})^2+((S_{12}^{PE}-S_{23}^{PM})^2-(S_{11}^{PE}-S_{11}^{PM})(S_{11}^{PE}-S_{33}^{PM}))\chi^2)\\
&\quad -S_{11}^{PM}S_{33}^{PM}-(2S_{23}^{PM}(-S_{12}^{PE}+S_{23}^{PM})-2S_{11}^{PM}S_{33}^{PM}+S_{11}^{PE}(S_{11}^{PM}+S_{33}^{PM}))\chi
\end{aligned}$$

The ME charge coefficient is obtained by solving the system of equations (27)–(41) and the average electric field equal to zero ($E^{avg} = 0$)

$$\begin{aligned}
\beta_{LT} &= \frac{d_{31}^{PE}(\chi-1)\chi(C_2)}{(1-\chi)(D_2)+\frac{\chi}{\epsilon_{11}^{PM}}(E_2+\epsilon_{33}^{PE}((S_{23}^{PM})^2-S_{11}^{PM}S_{33}^{PM}-F_2+G_2))} \qquad (43)\\
C_2 &= q_{33}^{PM}(S_{11}^{PM}-S_{23}^{PM}+(S_{11}^{PE}-S_{12}^{PE}-S_{11}^{PM}+S_{23}^{PM})\chi)\\
&\quad q_{31}^{PM}(S_{33}^{PM}+S_{23}^{PM}(\chi-1)-(-S_{11}^{PE}+S_{12}^{PE}+S_{33}^{PM})\chi)\\
D_2 &= (S_{23}^{PM})^2-S_{11}^{PM}S_{33}^{PM}+((S_{12}^{PE}-S_{23}^{PM})^2-(S_{11}^{PE}-S_{11}^{PM})(S_{11}^{PE}-S_{33}^{PM}))\chi^2\\
&\quad -(2S_{23}^{PM}(-S_{12}^{PE}+S_{23}^{PM})-2S_{11}^{PM}S_{33}^{PM}+S_{11}^{PE}(S_{11}^{PM}+S_{33}^{PM}))\chi\\
E_2 &= (d_{31}^{PE})^2\chi(S_{11}^{PM}-2S_{23}^{PM}+S_{33}^{PM}-(-2S_{11}^{PE}+2S_{12}^{PE}+S_{11}^{PM}-2S_{23}^{PM}+S_{33}^{PM})\chi)\\
F_2 &= (2S_{23}^{PM}(-S_{12}^{PE}+S_{23}^{PM})-2S_{11}^{PM}S_{33}^{PM}+S_{11}^{PE}(S_{11}^{PM}+S_{33}^{PM}))\chi\\
G_2 &= ((S_{12}^{PE}-S_{23}^{PM})^2-(S_{11}^{PE}-S_{11}^{PM})(S_{11}^{PE}-S_{33}^{PM}))\chi^2
\end{aligned}$$

The results obtained by this model are compared with the experimental work reported in [29]. The materials used for the PM and PE phase are FeBSiC and (001) PZN-PT, with properties listed in Table 2. Values for S_{12}^{PE}, S_{12}^{PM} and S_{23}^{PM} were calculated by assuming $\nu_{12}^{PE} = \nu_{12}^{PM} = \nu_{31}^{PM} = 1/3$, where ν is the Poisson ratio ($S_{12} = -\nu_{12}S_{11}$ and $S_{23}^{PM} = -\nu_{31}^{PM}S_{33}^{PM}$).

Material Property	FeBSiC	PZN-PT	Units
S_{11}	125	69	$10^{-12}m^2N^{-1}$
S_{33}	40	119	$10^{-12}m^2N^{-1}$
S_{12}	-42^a	-23^a	$10^{-12}m^2N^{-1}$
S_{23}	-13^a		$10^{-12}m^2N^{-1}$
ϵ/ϵ_0	see text	5500	
μ/μ_0	2	1	
d_{31}	0	-2800	$10^{-12}CN^{-1}$
q_{31}	-5800	0	$10^{-12}mA^{-1}$
q_{33}	12000	0	$10^{-12}mA^{-1}$

Table 2: Material Properties of PZN-PT ($Pb(Zn_{1/3}, Nb_{2/3})O_3 - 7\%PbTiO_3$) and FeBSiC from [29]. ^{a} were calculated by assuming $\nu_{12}^{PE} = \nu_{12}^{PM} = \nu_{23}^{PM} = 1/3$

The ME charge coefficient reported in [29] and the predictions obtained using different values for the relative dielectric permittivity of the PM phase are shown in Figure 6. When $\epsilon^{PM}/\epsilon_0 = 10$ is used, the calculated ME charge coefficient ($\chi = 0.33$) is $7.1 \times 10^{-9} C\, A^{-1} m^{-1}$, which is quite smaller than the experimentally measured value ($168 \times 10^{-9} C\, A^{-1} m^{-1}$). As previously discussed, this is due to the electric field produced in the PM phase. When the ME charge coefficient is calculated using higher values for the relative dielectric permittivity of the PM phase, β increases and the electric field in the PM phase decreases. It can be seen that the values converge to a single line. No difference is observed for $\epsilon^{PM}/\epsilon_0 > 10^6$, and the electric field in the PM phase $E \to 0$. This indicates that using a high relative dielectric permittivity is a valid approach to to take into account the high conductivity of the PM phase. Furthermore, the calculated ME charge coefficient ($201 \times 10^{-9} C\, A^{-1} m^{-1}$) when the electric field in the PM phase approaches zero, is in reasonable agreement with experimental data reported in [29] ($168 \times 10^{-9} C\, A^{-1} m^{-1}$).

The results obtained when the electric field in the PM phase is zero show that the ME charge coefficient increases when the PM volume fraction increases. This is due to the fact that higher amounts of PM phase will produce higher strain in the PE phase, resulting in a higher electric displacement in the PE phase. Since the electric displacement D does not depend on the PE phase thickness, no decrease in ME charge coefficient can be seen when higher amount of PM phase is used.

Using $\epsilon^{PM} \to \infty$, the expressions for the ME charge coefficient, in TT and LT configurations, reduce to

$$\beta_{TT} = \frac{(2d_{31}^{PE}\mu_{33}^{PE}q_{31}^{PM}(\chi-1)\chi)}{E_1} \tag{44}$$

$$E_1 = (1-\chi)(2(q_{31}^{PM})^2(\chi-1)^2 - (\mu_{33}^{PM}(\chi-1) - \mu_{33}^{PE}\chi) (S_{11}^{PM}(\chi-1) + S_{12}^{PM}(\chi-1) - (S_{11}^{PE} + S_{12}^{PE})\chi))$$

$$\beta_{LT} = \frac{d_{31}^{PE}(\chi-1)\chi C_2}{(1-\chi)D_2} \tag{45}$$

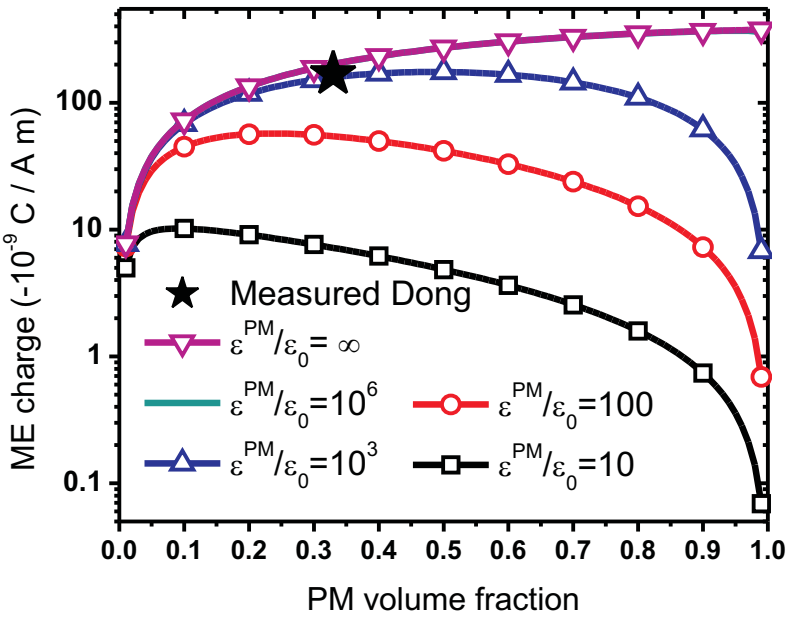

Figure 6: ME charge coefficient (LT) of the laminated FeBSiC-PZN-PT composite for different PM relative dielectric permittivities compared with the experimental result obtained by Dong *et al.* [29].

2.3 TL configuration

A similar approach is used to obtain the ME charge and voltage coefficient for the TL configuration, as follows

$$\begin{aligned}
\alpha_{TL} &= \frac{A_3}{B_3} \qquad (46)\\
A_3 &= -(\mu_{11}^{PE} q_{31}^{PM} \chi(-(d_{31}^{PE} + d_{33}^{PE})(S_{11}^{PM} - S_{12}^{PM}) + (d_{33}^{PE}(-S_{11}^{PE} + S_{23}^{PE} + S_{11}^{PM}\\
&\quad -S_{12}^{PM}) + d_{31}^{PE}(S_{23}^{PE} - S_{33}^{PE} + S_{11}^{PM} - S_{12}^{PM}))\chi))\\
B_3 &= \epsilon_{33}^{PE}((q_{31}^{PM})^2(\chi-1)^2(-2S_{11}^{PM}(\chi-1) + 2S_{12}^{PM}(\chi-1) + (S_{11}^{PE} - 2S_{23}^{PE}\\
&\quad +S_{33}^{PE})\chi) + (\mu_{33}^{PM}(\chi-1) - \mu_{11}^{PE}\chi)((S_{11}^{PM})^2(\chi-1)^2 - (S_{12}^{PM})^2(\chi-1)^2\\
&\quad -(S_{11}^{PE} + S_{33}^{PE})S_{11}^{PM}(\chi-1)\chi + 2S_{23}^{PE}S_{12}^{PM}(\chi-1)\chi + (-(S_{23}^{PE})^2 + S_{11}^{PE}S_{33}^{PE})\chi^2))\\
&\quad +\chi((d_{33}^{PE})^2(-(q_{31}^{PM})^2(\chi-1)^2 + (\mu_{33}^{PM}(\chi-1) - \mu_{11}^{PE}\chi)(S_{11}^{PM}(\chi-1) - S_{11}^{PE}\chi))\\
&\quad +2d_{31}^{PE}d_{33}^{PE}((q_{31}^{PM})^2(\chi-1)^2 - (\mu_{33}^{PM}(\chi-1) - \mu_{11}^{PE}\chi)(S_{12}^{PM}(\chi-1) - S_{23}^{PE}\chi))\\
&\quad +(d_{31}^{PE})^2(-(q_{31}^{PM})^2(\chi-1)^2 + (\mu_{33}^{PM}(\chi-1) - \mu_{11}^{PE}\chi)(S_{11}^{PM}(\chi-1) - S_{33}^{PE}\chi)))
\end{aligned}$$

and

$$\begin{aligned}
\beta_{TL} &= \frac{C_3}{D_3} \qquad (47)\\
C_3 &= -(\mu_{11}^{PE} q_{31}^{PM}(\chi-1)\chi(-(d_{31}^{PE} + d_{33}^{PE})(S_{11}^{PM} - S_{12}^{PM}) + (d_{33}^{PE}\\
&\quad (-S_{11}^{PE} + S_{23}^{PE} + S_{11}^{PM} - S_{12}^{PM}) + d_{31}^{PE}(S_{23}^{PE} - S_{33}^{PE} + S_{11}^{PM} - S_{12}^{PM}))\chi))\\
D_3 &= (q_{31}^{PM})^2(\chi-1)^2(-2S_{11}^{PM}(\chi-1) + 2S_{12}^{PM}(\chi-1) + (S_{11}^{PE} - 2S_{23}^{PE} + S_{33}^{PE})\chi)\\
&\quad +(\mu_{33}^{PM}(\chi-1) - \mu_{11}^{PE}\chi)((S_{11}^{PM})^2(\chi-1)^2 - (S_{12}^{PM})^2(\chi-1)^2\\
&\quad -(S_{11}^{PE} + S_{33}^{PE})S_{11}^{PM}(\chi-1)\chi + 2S_{23}^{PE}S_{12}^{PM}(\chi-1)\chi + (-(S_{23}^{PE})^2 + S_{11}^{PE}S_{33}^{PE})\chi^2)
\end{aligned}$$

2.4 LL configuration

A similar approach is used to obtain the ME charge and voltage coefficient for the LL configuration, obtaining

$$\begin{aligned}
\alpha_{LL} &= \frac{A_4}{B_4} \qquad (48)\\
A_4 &= \chi(d_{33}^{PE}(q_{33}^{PM}(S_{11}^{PM}(\chi-1) - S_{11}^{PE}\chi) + q_{31}^{PM}(S_{23}^{PM} + S_{23}^{PE}\chi - S_{23}^{PM}\chi))\\
&\quad +d_{31}^{PE}(q_{31}^{PM}(S_{33}^{PM}(\chi-1) - S_{33}^{PE}\chi) + q_{33}^{PM}(S_{23}^{PM} + S_{23}^{PE}\chi - S_{23}^{PM}\chi)))\\
B_4 &= \chi((d_{33}^{PE})^2(S_{11}^{PM}(\chi-1) - S_{11}^{PE}\chi) + (d_{31}^{PE})^2(S_{33}^{PM}(\chi-1) - S_{33}^{PE}\chi)\\
&\quad +2d_{31}^{PE}d_{33}^{PE}(S_{23}^{PM} + S_{23}^{PE}\chi - S_{23}^{PM}\chi)) + \epsilon_{33}^{PE}(-(S_{23}^{PM})^2(\chi-1)^2\\
&\quad +2S_{23}^{PE}S_{23}^{PM}(\chi-1)\chi + S_{11}^{PM}(S_{33}^{PM} + S_{33}^{PE}\chi) + \chi((S_{11}^{PE}\\
&\quad -2S_{11}^{PM})S_{33}^{PM} - (S_{23}^{PE})^2\chi + (S_{11}^{PE} - S_{11}^{PM})(S_{33}^{PE} - S_{33}^{PM})\chi))
\end{aligned}$$

and

$$\begin{aligned}
\beta_{LL} &= \frac{C_4}{D_4} \qquad (49)\\
C_4 &= (\chi-1)\chi(d_{33}^{PE}(q_{33}^{PM}(S_{11}^{PM}(\chi-1)-S_{11}^{PE}\chi)+q_{31}^{PM}(S_{23}^{PM}+S_{23}^{PE}\chi-S_{23}^{PM}\chi))\\
&\quad +d_{31}^{PE}(q_{31}^{PM}(S_{33}^{PM}(\chi-1)-S_{33}^{PE}\chi)+q_{33}^{PM}(S_{23}^{PM}+S_{23}^{PE}\chi-S_{23}^{PM}\chi)))\\
D_4 &= -(S_{23}^{PM})^2(\chi-1)^2+2S_{23}^{PE}S_{23}^{PM}(\chi-1)\chi+S_{11}^{PM}(S_{33}^{PM}+S_{33}^{PE}\chi)\\
&\quad +\chi((S_{11}^{PE}-2S_{11}^{PM})S_{33}^{PM}-(S_{23}^{PE})^2\chi+(S_{11}^{PE}-S_{11}^{PM})(S_{33}^{PE}-S_{33}^{PM})\chi)
\end{aligned}$$

In the LL configuration, the magnetic field goes through both phases. The electric field is confined to the PE phase by insulating the PM phase, otherwise no voltage or charge could be harvested as it would be dissipated in the conductive PM phase. The equations reflect the prescence of the insulator.

3 ME coupling Factor

The ME coupling factor is the ratio between the electrical work generated and magnetic work applied (or magnetic work generated and electrical work applied). It is an useful property to compare different ME composites in their ability to be used as energy transducers. The mathematical definition is the following

$$\kappa^2 = \frac{W_E^G}{W_M^A} \qquad (50)$$

where W_E^G is the electric work generated, and W_M^A is the magnetic work applied. The ME coupling factor can be expressed as a function of the ME charge coefficient and the electric and magnetic properties of the composite.

If a magnetic field is applied to the composite when it is short circuited ($E_3^{I->II}=0$), no electric work will be generated and magnetic work will be applied with the following magnitude (state I to state II in Figure 7)

$$W_M^A = \frac{B_z^{II}\times H_z^{II}}{2}\Big]_{E=0} = \frac{\mu_{zz}(H_z^{II})^2}{2}\Big]_{E=0} = \frac{\mu_{zz}^E(D_z^{II})^2}{2(\beta_{zz})^2} \qquad (51)$$

where μ_{zz}^E is the magnetic permeability in the z-direction of the composite measured at constant electric field and $\beta = \frac{D}{H}\big]_{E=0}$. Prior to the removal of the magnetic field the composite is open-circuited. From the state II to the state III, there is no electric work generated and the generated magnetic work is wasted. After this it is connected to an ideal electric load to complete the cycle. From the state III to the state I only electric work is generated. The amount of work generated is

$$\begin{aligned}
W_E^G &= \frac{D_z^{III}\times E_z^{III}}{2}\Big]_{H=0} \qquad (52)\\
&= \frac{(D_z^{III})^2}{2\epsilon_{zz}}\Big]_{H=0} = \frac{(D_z^{III})^2}{2\epsilon_{zz}^H} = \frac{(D_z^{II})^2}{2\epsilon_{zz}^H} \qquad (53)
\end{aligned}$$

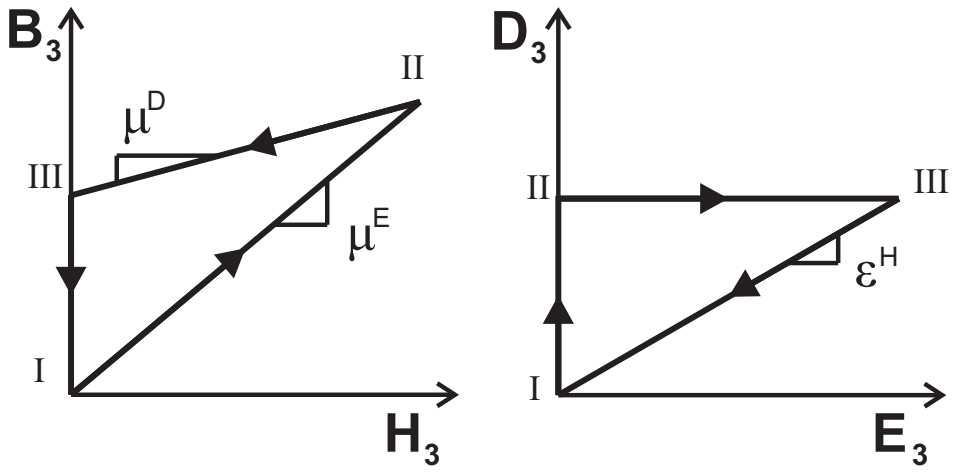

Figure 7: B-H and D-E diagram used to calculate the magnetic and electric work defined in ME coupling factor.

where ϵ_{zz}^H is the dielectric permittivity in the z-direction of the composite measured at constant magnetic field. With these values the ME coupling factor can be calculated as

$$\kappa_{zz}^2 = \frac{(D_z^{II})^2}{2\epsilon_{zz}^H}\frac{2(\beta_{zz})^2}{\mu_{zz}^E(D_z^{II})^2} = \frac{(\beta_{zz})^2}{\epsilon_{zz}^H\mu_{zz}^E} \tag{54}$$

$$= \frac{(\alpha_{zz})^2\epsilon_{zz}^H}{\mu_{zz}^E} \tag{55}$$

taking into account that $\beta_{ij} = \frac{\alpha_{ij}}{\epsilon_{jj}^H}$. The reciprocal of the ME coupling factor can be calculated as

$$\kappa^2 = \frac{W_M^G}{W_E^A} = \frac{W_E^G}{W_M^A} \tag{56}$$

where W_M^G is the magnetic work generated, and W_E^A is the electric work applied. These two definitions are equivalent.

Similarly, κ_{ij} is obtained as

$$\kappa_{ij}^2 = \frac{(\beta_{ij})^2}{\epsilon_{jj}^H\mu_{ii}^E} = \frac{(\alpha_{ij})^2\epsilon_{jj}^H}{\mu_{ii}^E} \tag{57}$$

Where the subscripts i and j correspond to the polarization and magnetization selected (Transverse or Longitudinal). The dielectric permittivity at constant magnetic field and magnetic permeability at constant electric displacement of the composite has to be calculated for all the different configurations. To do this the simple formulas for parallel and series capacitors cannot be used because in this case, fixing the magnetic field has an influence on the dielectric permittivity. It can be seen in (2) that for the composite, whenever an electric field is applied to measure the dielectric permittivity, a strain is produced that results in the increase of the magnetic flux density or magnetic field. Therefore, to calculate the dielectric

permittivity of the composite, ϵ^H, a similar approach as the one used for the calculation of the ME voltage coefficient α must be used.

To calculate α, the ratio between the electric field and the magnetic field at a constant electric displacement was evaluated. In the case of ϵ^H, the ratio between the electric displacement and the electric field at constant magnetic field has to be calculated as follows

$$\epsilon_{ij}^{H} = \frac{D_i}{E_j}\Big]_{H=0} \tag{58}$$

Similarly the magnetic permeability is calculated

$$\mu_{ij}^{D} = \frac{B_i}{H_j}\Big]_{D=0} \tag{59}$$

For the TT configuration the following expression are obtained

$$\begin{aligned}
\epsilon_{zz}^{H} &= \frac{E_1}{F_1} \qquad (60)\\
E_1 &= -(\epsilon_{33}^{PM}\mu_{33}^{PM}(\frac{1}{\chi}-1)(\mu_{33}^{PM}(\chi-1)-\mu_{33}^{PE}\chi)(-((2(d_{31}^{PE})^2\chi)/(\chi-1))\\
&\quad +\epsilon_{33}^{PE}(S_{11}^{PE}+S_{12}^{PE}-S_{11}^{PM}-S_{12}^{PM}+(S_{11}^{PE}+S_{12}^{PE})/(\chi-1)\\
&\quad -(2(q_{31}^{PM})^2(\chi-1))(\mu_{33}^{PM}+\mu_{33}^{PE}\chi-\mu_{33}^{PM}\chi))))\\
F_1 &= (\mu_{33}^{PM}(\frac{1}{\chi}-1)(\epsilon_{33}^{PM}(\chi-1)-\epsilon_{33}^{PE}\chi)(\mu_{33}^{PM}(S_{11}^{PM}+S_{12}^{PM})+2(q_{31}^{PM})^2(\chi-1)\\
&\quad +(\mu_{33}^{PE}-\mu_{33}^{PM})(S_{11}^{PM}+S_{12}^{PM})\chi)-\mu_{33}^{PM}(\mu_{33}^{PM}(\chi-1)-\mu_{33}^{PE}\chi)(2(d_{31}^{PE})^2\chi\\
&\quad +(S_{11}^{PE}+S_{12}^{PE})(\epsilon_{33}^{PM}(\chi-1)-\epsilon_{33}^{PE}\chi)))
\end{aligned}$$

and

$$\begin{aligned}
\mu_{zz}^{D} &= \frac{G_1}{H_1} \qquad (61)\\
G_1 &= (\mu_{33}^{PE}\mu_{33}^{PM}(1+(2\mu_{33}^{PE}(q_{31}^{PM})^2(\frac{1}{\chi}-1)\chi(\epsilon_{33}^{PM}+\epsilon_{33}^{PE}\chi\\
&\quad -\epsilon_{33}^{PM}\chi))/(\mu_{33}^{PM}(\frac{1}{\chi}-1)(\epsilon_{33}^{PM}(\chi-1)-\epsilon_{33}^{PE}\chi)(\mu_{33}^{PM}(S_{11}^{PM}+S_{12}^{PM})\\
&\quad +2(q_{31}^{PM})^2(\chi-1)+(\mu_{33}^{PE}-\mu_{33}^{PM})(S_{11}^{PM}+S_{12}^{PM})\chi)-\mu_{33}^{PM}(\mu_{33}^{PM}(\chi-1)\\
&\quad -\mu_{33}^{PE}\chi)(2(d_{31}^{PE})^2\chi+(S_{11}^{PE}+S_{12}^{PE})(\epsilon_{33}^{PM}(\chi-1)-\epsilon_{33}^{PE}\chi)))))\\
H_1 &= (\mu_{33}^{PM}+\mu_{33}^{PE}\chi-\mu_{33}^{PM}\chi)
\end{aligned}$$

In (60), when $\epsilon^{PM} \to \infty$, the electric field in the PM phase vanishes, i.e., $E^{PM} \to 0$, which is consistent with the actual phenomena inside the conductive PM phase. Therefore, this technique can be applied to calculate any property of the composite; in this case, dielectric permeability. Expanding E_1 and F_1 in (60), one can verify that ϵ^{PM} appears in both the numerator and denominator, in such a way that when $\epsilon^{PM} \to \infty$, they cancel out.

Expressions for the LT, TL and LL configurations can be obtained by following the same procedure. These expressions and all the coefficients calculated in this work are provided in MATLAB® and Scilab© format in the Website [27].

4 Demagnetizing Factor

As it was previously discussed in the introduction, when a structure is exposed to an external magnetic field (H_0) the internal magnetic field is reduced by the demagnetization field,

$$H_3 = H_0 + H_d = H_0 - N_3 M \tag{62}$$

where H_d is the demagnetizing field, N_3 is the demagnetizing factor in direction 3, and M is the magnetization. The magnetization can be written as follows,

$$M = \frac{H_0(\mu_r - 1)}{1 + N_3(\mu_r - 1)} \tag{63}$$

resulting in,

$$H_3 = H_0\Big(1 - \frac{N_3(\mu_r - 1)}{1 + N_3(\mu_r - 1)}\Big) \tag{64}$$

The demagnetizing factor has values between 0 and 1. When $N_3 = 0$ then $H_3 = H_0$ and when $N_3 = 1$ then $H_3 = \frac{H_0}{\mu_r}$. The composite structures with high demagnetizing factor and high relative permeability will show the highest reduction of internal magnetic field (H_3). This is relevant if one wishes to measure the extrinsic performance of the device, i.e., the voltage generated for a given magnetic field and specific device dimensions. However, the intrinsic material performance is independent of geometry. The extrinsic performance can be calculated combining the intrinsic material properties, as reported in this work, and the demagnetizing factor for particular device dimensions [30, 31].

The demagnetizing factor is given by the geometry of the structure, the simplest case is the sphere were $N_i = 1/3$ in all three directions and it has a constant value. It has to be noticed that the demagnetization factor has to satisfy the following condition, $N_1+N_2+N_3 = 1$. In the case of an infinite plate the out of plane demagnetizing factor is 1 and the in-plane demagnetizing factor is 0. The demagnetizing factor for non-infinite plates depends on the position and can be calculated using the equations derived by Joseph and Schlomann or the averaged demagnetization factor can be obtained using the expressions derived by Aharoni [30, 31].

In this work the demagnetizing effect is not considered because it is an extrinsic effect. The intrinsic magnetoelectric coefficients reported in this work are independent of the geometrical dimensions of the composite, thus simplifying the preliminary design and material selection criteria. Then, the dimensions of the magnetoelectric composite can be optimized taking into account the demagnetizing factor N_3. The optimal dimensions would yield $N_3 \to 0$.

For the case of the composites with longitudinal magnetization (§2.2 and §2.4), the thickness has to be considerably smaller than the in-plane dimensions to achieve $N = 0$.

For composites with transverse magnetization (§2.1 and §2.3), measured performance, rather than intrinsic performance, may be significantly reduced due to high demagnetization factor [32]. However, one could stack a number of ME laminates to build a device with high thickness-to-width ratio, $h >> w$, so that the device approximates a cylindrical rod, which has N=0 along the axis of the rod. Each ME laminate (that is, each PM/PE pair) must be thin to reduce the shear lag effect [23].

Material Property	Terfenol-D	PZT-5H	Units
S_{11}	44	16.5	$10^{-12}m^2N^{-1}$
S_{33}	38	20.7	$10^{-12}m^2N^{-1}$
S_{12}	-11	-4.78	$10^{-12}m^2N^{-1}$
S_{23}	-16.5	-8.45	$10^{-12}m^2N^{-1}$
ϵ_{33}/ϵ_0	∞	3400	
μ_{11}/μ_0	8.1	1	
μ_{33}/μ_0	3	1	
d_{31}	0	-274	$10^{-12}CN^{-1}$
d_{33}	0	593	$10^{-12}CN^{-1}$
q_{31}	-4300	0	$10^{-12}mA^{-1}$
q_{33}	8500	0	$10^{-12}mA^{-1}$
k_{31}	0.33	0.39	$10^{-12}CN^{-1}$
k_{33}	0.71	0.75	$10^{-12}CN^{-1}$

Table 3: Material Properties of PZT-5H and Terfernol-D from [33, 34].

5 Results

The expected application of the ME composite dictates which ME property needs to be optimized. For sensors, there are two different sensitivities: short circuit sensitivity and open circuit sensitivity. Higher short circuit sensitivity requires a higher ME charge coefficient β. Higher open circuit sensitivity requires a higher ME voltage coefficient α. For energy transducers, such as magnetic harvesters, a high κ is desired because in that case more electrical work will be generated for the same amount of magnetic work harvested.

Results are presented for PZT-5H/Terfenol-D. The properties of PZT-5H are obtained from Morgan Electro Ceramics [33]. The selected elastic properties are measured at constant electric field.

It is important to use the appropriate elastic properties in the analysis. Otherwise, significant errors may occur. For example, the compliance in the polarization direction of PZT-5H is $S_{33}^E = 20.7 \times 10^{-12} m^2 N^{-1}$ at constant electric field while it is only $S_{33}^D = 8.9 \times 10^{-12} m^2 N^{-1}$ at constant electric displacement. The same applies to the dielectric permittivity, but in this case it should be measured at constant stress. The magnetic permeability μ^E of the PE phase is required for the calculations, but it is immaterial if it is measured at constant electric field or constant electric displacement because there is no PM coupling in the PE phase. Since the magnetic permeability of PZT-5H is not reported in [33], a value $\mu/\mu_0 = 1$ is used for the examples in this study.

Additionally, all the properties have to be measured with the same polarization since the properties change drastically with different polarization intensities and direction. For the PM phase, Terfenol-D is selected and the properties were obtained from [34]. The values of these properties are reported in Table 3.

The analytical expression for the ME coupling factor for the different configurations are evaluated with the properties from Table 3. The maximum value of the ME coupling factor is κ =0.36 for the LL configuration and a PM volume fraction of 73%, as shown in Figure

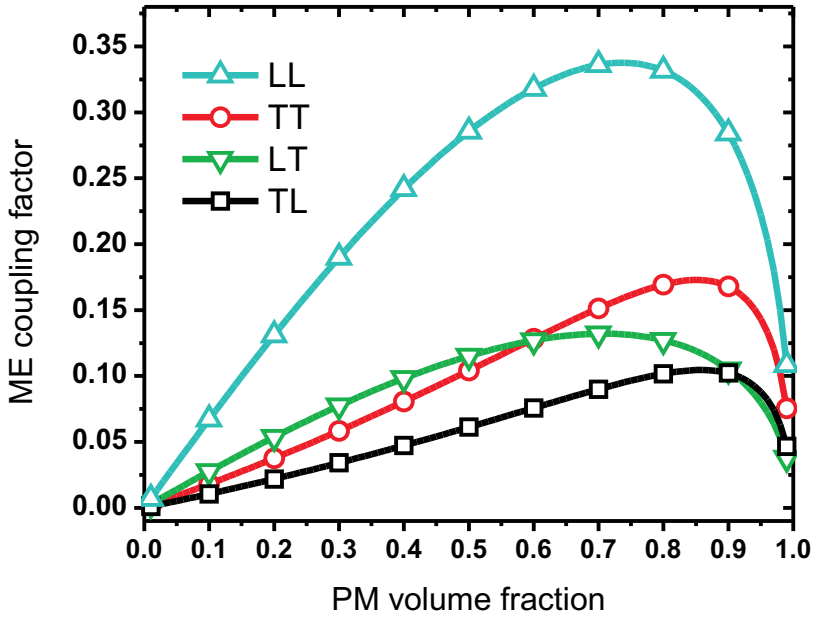

Figure 8: ME coupling factor of PZT-5H Terfenol-D composite for different PM volume fractions using TT, LT, TL and LL configurations.

8. The ME coupling factor as a function of PM volume fraction χ has a parabolic shape. This is due to the fact that for small χ the magnetic work applied cannot be transformed to mechanical work and for χ close to 1 the mechanical work generated by the PM phase cannot be converted to electrical work because the PE phase is too thin. The maximum ME coupling factor is obtained for the LL configuration because in that configuration the highest PE and PM coupling factors (k_{33}) of the constituents are being used.

The ME charge coefficients β for the different configurations can be seen in Figure 9. For the TT and LT configuration, β increases with increasing PM volume fraction. When higher χ is used, the stress in the PE phase increases resulting in a higher electric displacement. Taking into account that the PE area does not change, the electric displacement on the PE phase is the total electric displacement.

In the case of the LL and TL, the ME charge coefficient display a compromise between strain and the thickness of the PE phase. For small PM volume fraction, the increase of χ increases the strain resulting in a higher electric displacement and higher β. For high PM volume fraction χ, the electric displacement in the PE phase increases, but since the area of the PE phase is reduced, the average electric displacement of the laminate decreases.

The highest value of ME charge ($\beta_{TT} = 192 \times 10^{-9} CA^{-1}m^{-1}$) is obtained for the TT configuration using a PM volume fraction close to 1. The transverse polarization has the highest charge because it has the highest effective area. In the case of magnetization, the highest charge is expected for the longitudinal magnetization (LT) because $q_{33} > q_{31}$. But this is not the case because when the magnetic field is applied, an expansion in the y-direction

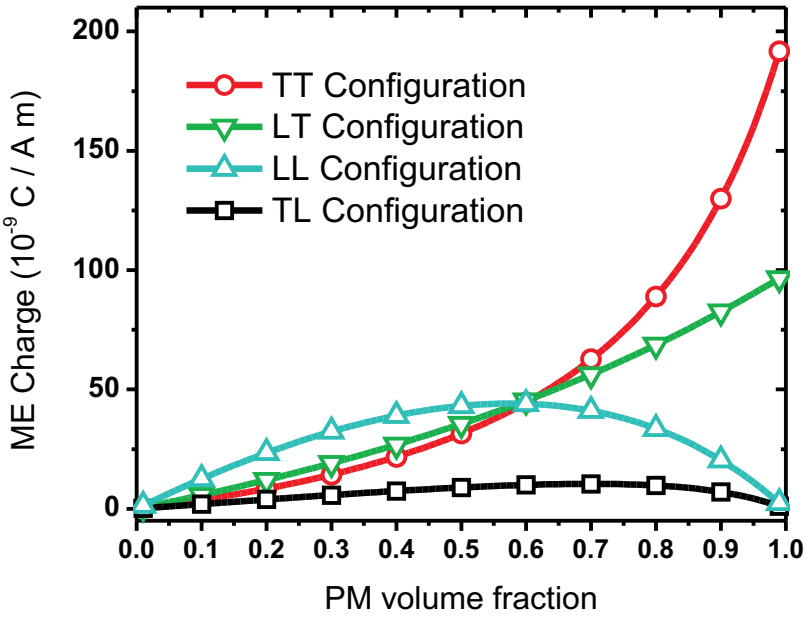

Figure 9: ME charge coefficient of PZT-5H Terfenol-D composite for different PM volume fractions using TT, LT, TL and LL configurations.

and a contraction in the x-direction take place. While, the expansion in the y-direction yields a negative electric displacement, the contraction in the x-direction yields a positive electric displacement, resulting in a small total electric displacement. Therefore, transverse magnetization results in higher charge because in this later case the electric displacement produced by the strain in the x and y-direction are equal.

The optimum β is obtained for volume fractions close to 1. The use of volume fractions close to 1 will result in a small ME coupling factor. This means that if the detector used to measure charge does not have an infinite resistance, the measured charge will be diminished. For this reason, is convenient to use a lower PM volume fraction, say at 90%, which yields a good ME charge coefficient ($130 \times 10^{-9} C\, A^{-1} m^{-1}$) and good ME coupling factor (0.17).

The ME voltage coefficient for PZT-5H/Terfenol-D composite is shown in Figure 10. It shows a trend similar to that of the ME charge coefficient, but since the total electric field increases with the thickness of the PE phase, the configurations with transverse polarization (TT and LT) are the ones to show a parabolic response – not the ones with longitudinal polarization. The LL configuration shows the highest ME voltage coefficient of $\alpha_{LL} = 18 V A^{-1}$ with $\chi \to 1$. In the LL configuration, the electric field due to contraction/expansion in the x and y-direction have the same sign because in this case the PE phase is polarized in the y-direction. A PM volume fraction of 85% is more convenient to combine a high $\alpha = 10.7 V A^{-1}$ with a very high ME coupling factor of 0.32.

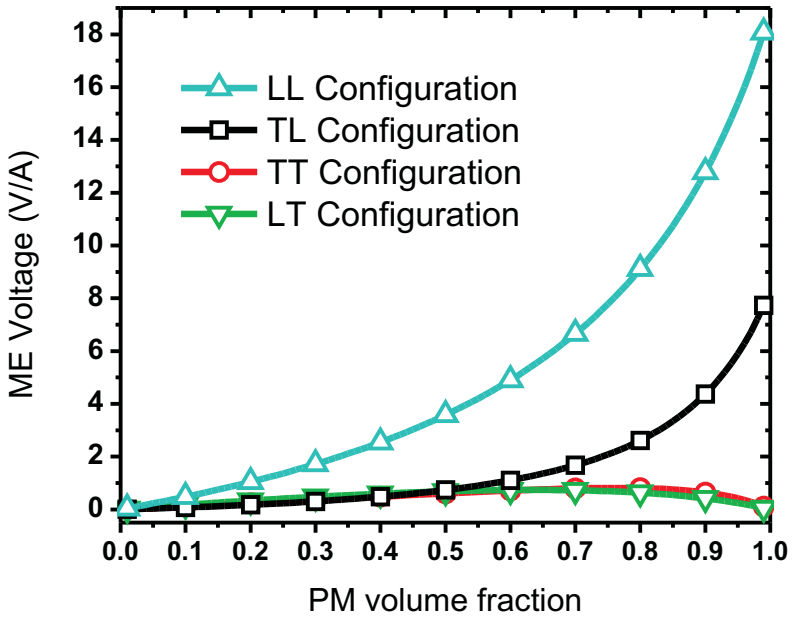

Figure 10: ME voltage coefficient of PZT-5H Terfenol-D composite for different PM volume fractions using TT, LT, TL and LL configurations.

6 Conclusions

A new method is proposed to take into account the high conductivity of the PM phase. The method consists of artificially increasing the electrical permittivity of the PM phase. From the analysis of three composites made with three PM and three PE materials, analyzed for PM volume fraction continuously varying from zero to one, we conclude that setting the relative permittivity of the PM to 10^9 is equivalent to a fully conducting PM material and thus a negligible electric field in the PM.

Artificially increasing the dielectric permittivity of the PM phase in the numerical calculation to simulate the high conductivity of said phase proved to be an expedient method for taking into account the conductivity of the PM material without having to introduce additional equations modeling electrical conductivity in the proposed model. In fact, as permittivity $\epsilon^{PM} \to \infty$, the ME charge coefficient vs. PM volume fraction plot becomes insensitivity to permittivity and the values predicted are close to experimental data for FeBSiC/PZN-PT (Fig. 6) for LT configuration. Also, the formulas become much simpler.

For the material systems analyzed, both ME voltage and charge coefficients are maximized when the PM volume fraction $\chi \to 1$ (in particular configurations). But such design is unrealistic because an infinitely thin layer of PE cannot generate any significant work. Thus, measuring the voltage or the current would be very difficult. In this regard, the newly developed ME coupling factor equations (54, 55, 57) prove to be very useful in that they provide an indication of the work conversion that can be achieved.

For Terfenol-D/PZT-5H in TT configuration, a reduction of PM volume fraction from

100% to 90% results in a reduction of ME charge coefficient from an upper bound of $192 \times 10^{-9} C\,A^{-1}m^{-1}$ down to $130 \times 10^{-9} C\,A^{-1}m^{-1}$, while the ME coupling factor increases from zero to 0.17. Note that a value of coupling factor κ =1.0, although practically unattainable, would indicate 100% work conversion.

In LL configuration, a reduction of PM volume fraction from 100% to 85% results in a reduction of ME voltage coefficient from an upper bound $\alpha = 18VA^{-1}$ down to $\alpha = 10.7VA^{-1}$, while the ME coupling factor increases from zero to 0.32. The formulas presented herein can be used to tune the volume fraction to achieve an acceptable compromise between ME charge, or voltage, and work conversion.

If work conversion needs to be maximized (for transducer applications), the optimum configuration is not TT but LL, at PM volume fraction 73%, yielding a ME coupling factor (i.e., conversion) of 0.36.

For accurate calculation, it is very important to use the appropriate elastic compliance of the material, which can vary significantly depending on the testing conditions. For example, the compliance in the polarization direction S_{33} of PZT-5H changes from 20.7×10^{-12} to $8.9 \times 10^{-12} m^2 N^{-1}$ when it is measured at constant E and constant D, respectively.

A trade off between voltage and PM volume fraction is evident for LSMO/PZT (Figure 3) yielding an optimum PM volume fraction χ =65 % in TT configuration. Optimum values like this are dependent on material properties and configuration. Therefore, it is of significant interest for preliminary design and material selection to count with a complete set of formulas such as those proposed in this manuscript to be able to assess voltage, charge, and energy conversion for any of the four laminated configurations, as function of material and geometrical parameters.

7 Acknowledgment

The authors wish to thank the Energy Materials Science and Engineering Program (EMSE) at West Virginia University for the financial and infrastructure support.

References

[1] S. Dong, J. Zhai, F. Bai, J.-F. Li, and D. Viehland, "Push-pull mode magnetostrictive/piezoelectric laminate composite with an enhanced magnetoelectric voltage coefficient," *Applied Physics Letters*, vol. 87, no. 6, p. 062502, 2005.

[2] J. Huang, R. O'Handley, and D. Bono, "New, high-sensitivity, hybrid magnetostrictive/electroactive magnetic field sensors," *Proceedings of SPIE - The International Society for Optical Engineering*, vol. 5050, pp. 229–237, 2003.

[3] S. Roundy and Y. Zhang, "Toward self-tuning adaptive vibration based microgenerators," *Proceedings of SPIE - The International Society for Optical Engineering*, vol. 5649, no. PART 1, pp. 373–384, 2005.

[4] P. Li, Y. Wen, and L. Bian, "Enhanced magnetoelectric effects in composite of piezoelectric ceramics, rare-earth iron alloys, and ultrasonic horn," *Applied Physics Letters*, vol. 90, no. 2, p. 022503, 2007.

[5] S. Dong, J. Zhai, J. F. Li, D. Viehland, and S. Priya, "Multimodal system for harvesting magnetic and mechanical energy," *Applied Physics Letters*, vol. 93, no. 10, p. 103511, 2008.

[6] I. Sari, T. Balkan, and H. Kulah, "An electromagnetic micro power generator for wideband environmental vibrations," *Sensors and Actuators, A: Physical*, vol. 145-146, no. 1-2, pp. 405–413, 2008.

[7] X. Dai, Y. Wen, P. Li, J. Yang, and G. Zhang, "Modeling, characterization and fabrication of vibration energy harvester using Terfenol-D/PZT/Terfenol-D composite transducer," *Sensors and Actuators A: Physical*, vol. 156, no. 2, pp. 350 – 358, 2009.

[8] S. D. Moss, J. E. McLeod, I. G. Powlesland, and S. C. Galea, "A bi-axial magnetoelectric vibration energy harvester," *Sensors and Actuators A: Physical*, vol. 175, no. 0, pp. 165 – 168, 2012.

[9] Z. Shi, C. Wang, X. Liu, and C. Nan, "A four-state memory cell based on magnetoelectric composite," *Chinese Science Bulletin*, vol. 53, no. 14, pp. 2135–2138, 2008.

[10] G. T. Rado and V. J. Folen, "Observation of the magnetically induced magnetoelectric effect and evidence for antiferromagnetic domains," *Physical review letters*, vol. 7, pp. 310–311, 1961.

[11] G. T. Rado, J. M. Ferrari, and W. G. Maisch, "Magnetoelectric susceptibility and magnetic symmetry of magnetoelectrically annealed $TbPO_4$," *Physical review B*, vol. 29, pp. 4041–4048, 1984.

[12] J. Ryu, S. Priya, A. V. Carazo, K. Uchino, and H.-E. Kim, "Effect of the magnetostrictive layer on magnetoelectric properties in lead zirconate titanate/terfenol- D laminate composites," *Journal of the American Ceramic Society*, vol. 84, no. 12, pp. 2905–2908, 2001.

[13] A. Lakhtakia and T. G. Mackay, "Meet the metamaterials," *Optics and Photonics*, vol. 1, pp. 32–39, 2007.

[14] S. Priya, J. Ryu, C.-S. Park, J. Oliver, J.-J. Choi, and D.-S. Park, "Piezoelectric and magnetoelectric thick films for fabricating power sources in wireless sensor nodes," *Sensors*, vol. 9, no. 8, pp. 6362–6384, 2009.

[15] R. Kambale, D.-Y. Jeong, and J. Ryu, "Current status of magnetoelectric composite thin/thick films," *Advances in Condensed Matter Physics*, 2012.

[16] G. Harshe, J. Dougherty, and R. Newnham, "Theoretical modelling of multilayer magnetoelectric composites," *International journal of applied electromagnetics in materials*, vol. 4, no. 2, pp. 145–159, 1993.

[17] C.-W. Nan, "Magnetoelectric effect in composites of piezoelectric and piezomagnetic phases," *Physical Review B*, vol. 50, pp. 6082–6088, 1994.

[18] I. Osaretin and R. Rojas, "Theoretical model for the magnetoelectric effect in magnetostrictive/ piezoelectric composites," *Physical Review B - Condensed Matter and Materials Physics*, vol. 82, no. 17, 2010.

[19] M. Bichurin and V. Petrov, "Modeling of magnetoelectric interaction in magnetostrictive-piezoelectric composites," *Advances in Condensed Matter Physics*, 2012.

[20] Wolfram Research, "Mathematica 9.0," tech. rep., Wolfram Research, Champaign, Illinois, 2013.

[21] S. Dong, J.-F. Li, and D. Viehland, "Magnetoelectric coupling, efficiency, and voltage gain effect in piezoelectric-piezomagnetic laminate composites," *Journal of Materials Science*, vol. 41, no. 1, pp. 97–106, 2006.

[22] K. Sun and Y. Kim, "Design of magnetoelectric multiferroic heterostructures by topology optimization," *Journal of Physics D: Applied Physics*, vol. 44, no. 18, 2011.

[23] C.-M. Chang and G. Carman, "Modeling shear lag and demagnetization effects in magneto-electric laminate composites," *Physical Review B - Condensed Matter and Materials Physics*, vol. 76, no. 13, 2007.

[24] C.-M. Chang and G. Carman, "Experimental evidence of end effects in magneto-electric laminate composites," *Journal of Applied Physics*, vol. 102, no. 12, 2007.

[25] E. Barbero, *Finite element analysis of composite materials*. Composite Materials: Analysis and Design Series, Boca Raton, FL: Taylor and Francis, 2008.

[26] S. Dong, J. Zhai, J. Li, and D. Viehland, "Near-ideal magnetoelectricity in high-permeability magnetostrictive/ piezofiber laminates with a (2-1) connectivity," *Applied Physics Letters*, vol. 89, no. 25, 2006.

[27] Web resource, 2014. http://barbero.cadec-online.com/papers/source/ME/laminate/.

[28] J. Na, T. Lee, and S. Park, "Effects of cation distribution on the magnetic and electrical properties of cobalt ferrite," *IEEE Transactions on Magnetics*, vol. 28, no. 5 pt 2, pp. 2433–2435, 1992.

[29] S. Dong, J. Zhai, Z. Xing, J. Li, and D. Viehland, "Giant magnetoelectric effect (under a dc magnetic bias of 2 Oe) in laminate composites of $FeBSiC$ alloy ribbons and $Pb(Zn_{1/3}, Nb_{2/3})O_3$ -7 % $PbTiO_3$ fibers," *Applied Physics Letters*, vol. 91, no. 2, 2007.

[30] R. Joseph and E. Schlomann, "Demagnetizing field in nonellipsoidal bodies," *Journal of Applied Physics*, vol. 36, no. 5, pp. 1579–1593, 1965.

[31] A. Aharoni, "Demagnetizing factors for rectangular ferromagnetic prisms," *Journal of Applied Physics*, vol. 83, no. 6, pp. 3432–3434, 1998.

[32] E. Quandt, S. Stein, and M. Wuttig, "Magnetic vector field sensor using magnetoelectric thin-film composites," *IEEE Transactions on Magnetics*, vol. 41, no. 10, pp. 3667–3669, 2005.

[33] D. Berlincourt and H. H. A. Krueger, "Properties of morgan electro ceramic ceramics," tech. rep., Morgan Electro Ceramics.

[34] C. Sherman and J. Butler, *Transducers and Arrays for Underwater Sound*. The Underwater Acoustics Series, Springer, 2007.